3D bioprinting bioglass to construct vascularized full-thickness skin substitutes for wound healing

Yanyan Liu [a,b], Xin Liu [a,c,f,**], Haitao Guo [a,c,e], Xinhuan Wang [a,c], Ailing Li [d], Dong Qiu [d,e], Qi Gu [a,c,e,*]

[a] State Key Laboratory of Membrane Biology, Institute of Zoology, Chinese Academy of Sciences, Chaoyang District, Beijing, 100101, PR China
[b] School of Materials Design and Engineering, Beijing Institute of Fashion Technology, Chaoyang District, Beijing, 100029, PR China
[c] Beijing Institute for Stem Cell and Regenerative Medicine, Chaoyang District, Beijing, 100101, PR China
[d] Beijing National Laboratory for Molecular Sciences, State Key Laboratory of Polymer Physics and Chemistry, Institute of Chemistry, Chinese Academy of Sciences, Haidian District, Beijing, 100190, PR China
[e] University of Chinese Academy of Sciences, Huairou District, Beijing, 101449, PR China
[f] Key Laboratory of Organ Regeneration and Transplantation of the Ministry of Education, Jilin University, Changchun 130061, PR China

ARTICLE INFO

ABSTRACT

Constructing three-dimensional (3D) bioprinted skin tissues that accurately replicate the mechanical properties of native skin and provide adequate oxygen and nutrient support remains a formidable challenge. In this study, we incorporated phosphosilicate calcium bioglasses (PSCs), a type of bioactive glass (BG), into the bioinks used for 3D bioprinting. The resulting bioink exhibited mechanical properties and biocompatibility that closely resembled those of natural skin. Utilizing 3D bioprinting technology, we successfully fabricated full-thickness skin substitutes, which underwent comprehensive evaluation to assess their regenerative potential in treating full-thickness skin injuries in rats. Remarkably, the skin substitutes loaded with PSCs exhibited exceptional angiogenic activity, as evidenced by the upregulation of angiogenesis-related genes in vitro and the observation of enhanced vascularization in wound tissue sections in vivo. These findings conclusively demonstrated the outstanding efficacy of PSCs in promoting angiogenesis and facilitating the repair of full-thickness skin wounds. The insights garnered from this study provide a valuable reference strategy for the development of skin tissue grafts with potent angiogenesis-inducing capabilities.

1. Introduction

The skin is the largest human organ and plays important functions, including a protective barrier, temperature regulation, and the prevention of water loss [1]. Cutaneous wounds, especially the extensive full-thickness wounds that damage blood vessels, severely affect human life and health because cells in wounds suffer from hypoxia and nutritional deficiency [2–4]. While autografts are considered the "gold standard" approach for treating severe skin injuries, they are restricted by limitations such as donor site availability and morbidity [5,6]. Besides, the existing commercial skin substitutes have a great gap in vascular networks for nutrient delivery in full-thickness wounds [7,8]. Therefore, artificial skin substitutes are believed to provide significant advantages with desired cell composition and controlled geometrical morphology for vascularized skin reconstruction [9,10].

In recent years, 3D bioprinting has held great promise as an advanced technology for mimicking the complexity and heterogeneity of skin as it enables the precise deposition of various living cells and biomaterials [9,11–14]. More and more studies have suggested the potential of the printing technique in the biofabrication of skin substitutes containing keratinocytes and fibroblasts [15,16]. Nevertheless, vascularized 3D printed skin models are still far from native human skin because of the complex induction process and growth factor inactivation [17,18]. From the perspective of applications, skin grafts should not only accelerate wound healing but also provide appropriate mechanical strength and structural stability to avoid secondary surgery and

---

potential scarring risk [19,20]. Therefore, exploiting 3D printed skin substitutes that integrate angiogenic functions and biomimetic mechanical strength is urgently needed [21].

Recently, BG has been shown to stimulate angiogenesis in wound repair, which is attributable to the released ions [22–26]. Our previous studies have reported that PSC enabled the angiogenic activities of human umbilical cord vein endothelial cells (HUVECs) in gelatin methacryoyl (GelMA/GM) and fibrin based soft bioink [27]. However, the poor mechanical properties of GelMA and fibrin pose a compliance mismatch for engineered skin grafts. An attractive hypothesis is to develop a PSC-containing toughness hydrogel, which is expected to exhibit mechanical robustness and excellent angiogenic ability.

Herin, we present a vascularized full-thickness skin substitute comprised of interpenetrating polymer network (IPN) bioink and living cells by 3D printing the epidermal layer and the dermal layer, respectively. The sodium alginate (Alg) – gelatin (Gel) or Alg-GelMA IPN hydrogel was successfully prepared and showed toughness and mechanical properties. Subsequently, PSC employed Alg-GelMA IPN hydrogels, which were developed and exhibited appropriate mechanical properties, good biocompatibility, and induced vascularized bioactivity *in vitro*. The skin substitutes were generated by 3D printing an Alg-Gel hydrogel layer to mimic the epidermis and 3D printing an HUVECs and human umbilical cord mesenchymal stem cells (MSCs) encapsulated PSC-Alg-GelMA hydrogel layer to mimic the dermis. Moreover, we demonstrated a significant improvement in blood vessel formation, collagen deposition, and the applicability of these skin substitutes for skin reconstruction in full-thickness skin injury rat models.

2. Materials and methods

2.1. Materials

The main reagents used in this study were: sodium alginate (Alg, from brown algae, low viscosity, A1112, Sigma), sodium alginate (from brown algae, medium viscosity, 71,238, Sigma), gelatin (Gel, from porcine skin, G1890, Sigma), calcium chloride ($CaCl_2$, C5670, Sigma), glutamine transaminase (TG, G8661, Solarbio), phosphate buffered saline (PBS, 02-02402ACS, Biological Industries), endothelial cell growth medium-2 (complete EGM-2 BulletKit, CC3162, Lonza), fetal bovine serum (FBS, 10,099–141, Gibco), Dulbecco's modified eagle medium (DMEM, C11965500BT, Gibco), GlutaMAX (35,050,061, Thermo), minimum essential medium non-essential amino acids (MEM NEAA, 11,140,050, Gibco), penicillin-Streptomycin (SP, 60162ES76, Yeasen), trypsin-EDTA (25200072, Gibco), resazurin (R817239, Macklin), RNAiso Plus (9108, Takara), PrimeScript™ RT reagent Kit (RR047A, Takara), TB Green® Premix Ex Taq (RR420A, Takara), 4 % para-formaldehyde (P0099, Beyotime), bovineVKO9 serum albumin (BSA, SW3015, Solarbio), Triton X-100 (X100, Sigma), Live/Dead Viability Kit (L-3224, Life technologies). GelMA was prepared according to the method reported by Liu et al. [28]. PSCs were donated by Dong Qiu Group [29].

2.2. Bioink preparation

All bioinks were prepared in sterile conditions. To prepare the 2Alg15Gel hydrogel precursor, the powder was dissolved in 0.9 wt% saline to achieve a final concentration of 2 wt% sodium alginate and 15 wt% gelatin. To prepare the Alg/GM hydrogel precursors, the powder was mixed together to achieve a final concentration of 0, 1, 2, 3, 4, 5 wt% sodium alginate and 0, 1, 2, 3, 4, 5 wt% GelMA in 0.9 wt% saline. The Alg/GM/PSC composite hydrogel precursors were obtained by the addition of PSC powder (0, 1, 5, or 10 mg mL^{-1}). Hydrogels with alginate composition were ionic crosslinked by 2 wt% $CaCl_2$ at room temperature for 1 min. Hydrogels with gelatin or GelMA composition were enzyme crosslinked by 1 wt% TG solution at 37 °C for 4 h. Among them, the sodium alginate used is medium viscosity.

2.3. Scanning electron microscopy (SEM)

The hydrogels were cross-linked as mentioned in 2.2 and then immersed in PBS at 37 °C for 12 hours. For SEM analysis, the samples were freeze-fractured by immersion in liquid nitrogen for 60 s and sublimation at −75 °C for 90 minutes. Then, the samples were coated with Au for 80 s at 12 mA by a sputter and imaged with SEM (HITACHI S–3000 N&Quorum PP3000T). The pore diameter was measured using ImageJ.

2.4. Mechanical measurement

The poured samples were prepared by shaping the hydrogel into a dumbbell-shaped and cube-shaped mold. The printed and poured samples were cross-linked according to 2.2 above. The rectangle in the middle of the dumbbell-shaped sample was 15 mm in length, 2 mm in thickness, and 3 mm in width. Compressive samples were prepared in molds (5 mm in length and 2 mm in depth). Mechanical properties of hydrogels were measured on a universal tensile machine (Instron 5943, Norwood) fitted with a load cell capacity of 50 N. For the pure-shear test, the samples were loaded to maximum strain until broken using a strain rate of 10 mm min^{-1}, and the modulus of each sample was calculated from the slope of the stress-strain curve within the 25 % strain. For loading-unloading test, the samples were loaded to 25 % strain and unloaded using the same stretching rate. Regarding the compression test, it's important to note that the strain rate utilized was 1 mmmin^{-1}. The resulting compressive modulus was then approximately linearly fitted based on the stress-strain curve within the strain range of 10 %–25 %.

2.5. Rheological measurement

Rheological properties of hydrogels were quantified on a rheometer (MCR302, Anton Paar) using a 0.5° core plate geometry with a diameter of 25 mm and a gap height of 25 μm. Firstly, samples were equilibrated at 10 °C for 180 s before testing. Then, viscosities were measured using flow sweeps from shear rates of 0.01–1000 s^{-1}. Secondly, temperature sweeps were performed over the range from 0 to 40 °C using an oscillatory frequency of 1 Hz and a shear strain of 1 %.

2.6. Cell culture and maintenance

HUVECs and MSCs were isolated from fresh human umbilical cord (Approval Number: 2022-KY-074-01). Human foreskin fibroblasts (HFFs) were donated by the National Stem Cell Resource Center, Beijing. Briefly, 1×10^4 cells cm^{-2} were plated on tissue culture plastic and incubated at 37 °C and 5 % CO_2. HUVECs were expanded in EGM-2. HFFs and MSCs were maintained in DMEM supplemented with 15 % FBS, 1 % MEM NEAA, 1 % GlutaMAX, and 1 % SP. All the cells were not used beyond the tenth passage. The medium was changed at least every two days.

2.7. Cell proliferation assay

The effect of the concentration of PSC on the 2Alg3GM hydrogel on the proliferation of fibroblasts, MSCs, and HUVECs was assessed using resazurin according to the instructions. Firstly, the 2Alg3GM hydrogel precursors with different concentrations of PSC (0, 1, 5, 10 mg mL^{-1}) were prepared and spread evenly at the bottom of the 24-well plate (200 μL for each well). After being cross-linked as described in 2.2, HUVECs, MSCs, and HFFs were seeded on the surface of hydrogels at an initial density of 3×10^4 cells per well. Then, at days 1, 3, and 7, resazurin was diluted with media without growth factors and serum and added to each well. After another 4 h incubation at 37 °C, the absorbance values were recorded spectrophotometrically at wavelengths of 590 nm with a microplate reader.

2.8. Bioprinting process

The designed skin substitutes and dumbbell-shaped mold for 3D bioprinting were drawn using computer-aided design (CAD) software (SolidWorks, La Jolla, CA, USA). The bioprinting procedure was carried out on the SIA bioprinter as previously reported [28]. Before printing, all bioink solutions were centrifuged to remove air bubbles. Each ink was housed in a syringe equipped with a 300-μm diameter nozzle. The printing platform temperature was maintained at 4 °C.

To manufacture skin substitutes, 2Alg15Gel was used as the epidermis bioink and maintained at 37 °C before printing. 2Alg3GM with or without PSC was used as the dermis bioink. HUVECs and MSCs were dispersed in dermis bioink solution at 2×10^6 cells mL^{-1} and 1×10^6 cells mL^{-1}, respectively. The dermis bioink was maintained at 10 °C before printing. The printing speed was 10 mm s^{-1}, and the filment orientation was 60°. The dimensions of the cylindrical construct were 15 mm in diameter, with ten layers in height. The epidermis bioink printed four layers with 60 % infill rates, and the dermis bioink printed six layers with 30 % infill rates. To produce dumbbell-shaped molds for mechanical testing, the 2Alg3GM5PSC bioinks were centrifuged to remove air bubbles, and loaded into a syringe. The filment orientation was 0°, 30°, 60°, 90°, respectively. Finally, the printed skin substitutes and the dumbbell-shaped molds were cross-linked as described in 2.2.

2.9. Cell viability assay

Live/Dead Viability Kit was used to assess the bioactivity of HUVECs and MSCs following the manufacturer's protocol. Briefly, 2Alg15Gel and 2Alg3GM containing 0, 1, 5, 10 mg mL^{-1} PSC were used to print the full-thickness skin substitute as described in 2.8. After culturing in EGM-2 at 37 °C and 5 % CO$_2$ for 24 h, samples were stained using 2 μL mL^{-1} Calcein AM in PBS for 1 h and then stained using 1 μL mL^{-1} PI in PBS for 30 min. Finally, the samples were washed with PBS and imaged using a fluorescence microscope (Andor Dragonfly 505, UK).

2.10. Quantitative polymerase chain reaction (Q-PCR)

The samples were prepared as described in 2.8. After being cultured for 3 days, the samples were washed three times with cold PBS. RNAiso Plus was used to extract the total RNA from each sample. The concentrations of extracted RNA were measured with a spectrophotometer (DeNovix DS-11). cDNA was synthesized using a PrimeScript™ RT reagent kit according to the instructions. Q-PCR analysis was performed by a real-time PCR system (LightCycler 480II, USA) with TB Green® Premix Ex Taq. The primers of the chosen genes and GAPDH used in this experiment are listed in Table 1. The data were analyzed by the 2ˆ -ΔΔCt method.

2.11. In vivo wound healing assessment

SD (8–10 weeks) female rats were purchased from Charles River Laboratories (CRL, Beijing). The SD rats were raised under specific-pathogen-free conditions and handled following the guidelines of the Animal Care and Use Committee of the Institute of Zoology, Chinese Academy of Sciences (Ethical Approval No. IOZ20180063).

The printed full-thickness skin substitutes were cultured in an incubator at 37 °C and 5 % CO$_2$ for 2 days before transplantation. To create a full-thickness skin wound, a standardized circular defect (diameter = 15 mm) was created on both sides of each Sprague-Dawley (S-D) rat's dorsum using a sterile scalpel. Then, the full-thickness skin substitutes (+ cells + PSC group), the printed 2Alg3GM5PSC hydrogels with the epidermis layer (+ PSC group), or the printed 2Alg3GM hydrogels with the epidermis layer (hydrogel group) were placed on each skin defect. The wounds were bandaged with gauze and tape. At days 0, 3, 7, and 14 post-transplantation, the images of each wound were captured for wound area statistics, and one wound sample from each group was retrieved for histological and immunohistochemical analysis.

2.12. Immunofluorescence, histological and immunohistochemical analysis

For the immunofluorescence staining, the printed full-thickness skin substitutes were fixed in 4 % paraformaldehyde, permeabilized with Triton X-100, and blocked with BSA. Then, the samples were incubated with endothelial cell marker platelet and endothelial cell adhesion molecule 1 (CD31) primary antibody (ab24590, abcam) and followed by fluorescence-conjugated secondary antibodies Alexa Fluor 488 (A21202, Invitrogen) and 4′,6-diamidino-2-phenylindole (DAPI, G1012, Servicebio).

The wound tissues were fixed in 4 % paraformaldehyde for more than 24 hours. For hematoxylin and eosin (H&E) and Masson's trichrome staining, the samples were dehydrated, embedded in paraffin, and cut into 6-μm thick sections. The sections were stained with H&E or Masson's trichrome, and examined with an optical microscope.

For the immunohistochemical staining, the sections were rehydrated and incubated with the universal macrophage marker CD68 primary antibody (GB113109, Servicebio), the M2 phenotype of macrophage marker CD163 primary antibody (GB11340-1, Servicebio), collagen I (COL I) primary antibody solution (GB11022-3, Servicebio), CD31 primary antibody (GB11063, Servicebio), and alpha smooth muscle actin (α-SMA) primary antibody (GB111364, Servicebio) at 4 °C overnight. Subsequently, the sections were incubated with secondary antibody for 1 h at room temperature. DAB and hematoxylin were used to develop the color reaction. Finally, images were taken through microscope (Leica Aperio VESA8). The number of blood vessels was determined by counting 10 randomly selected areas according to the CD31 staining. The diameters of blood vessels were counted using ImageJ.

2.13. Statistical analysis

All data were processed in Origin Pro 2021 (GraphPad Software, USA) or GraphPad Prism 9.5.0 (OriginLab Corporation, USA). One-way ANOVA was used to determine statistical significance. ns, no significant difference. *, **, ***, and **** represent $p < 0.05$, $p < 0.01$, $p < 0.001$, and $p < 0.0001$, respectively.

3. Results

3.1. Designing and characterization of hydrogels for skin substitutes printing

The working concept for the full-thickness skin tissue is briefly depicted in Fig. 1. As Fig. 1A shown that we designed two bioinks for the construction of the epidermis and the dermis, respectively. And then Ca^{2+} and TG were used sequentially for crosslinking to form an interpenetrating polymer network with ionic and covalent bonds (Fig. 1B). Finally, the full-thickness skin tissue graft was used to repair full-thickness skin wounds with a diameter of about 15 mm which located on both sides of the rat's back (Fig. 1C).

To develop a bioink with satisfactory properties for printing skin substitutes, gelatin, sodium alginate, and GelMA were chosen as the main bodies of the bioinks for printing. 2 % medium viscosity sodium alginate (2Alg) was mixed with 15 % gelatin (15Gel) to achieve tough mechanical properties. It was found that the mixing of sodium alginate with gelatin would greatly improve the elongation at break (Fig. 2A) and the Young's modulus (Figs. 2C and 15Gel: 42.182 kPa, 2Alg15Gel: 194.234 kPa). To create the interpenetrating polymer network hydrogels combining good biocompatibility with appropriate mechanical properties, 2 % middle-viscosity sodium alginate (2MAlg) and low-viscosity sodium alginate (2LAlg) were mixed with 3 % GelMA (3 GM), respectively. As the result and the statistics separately showed in Fig. 2B and C, the Young's modulus of 2MAlg3GM was much higher than
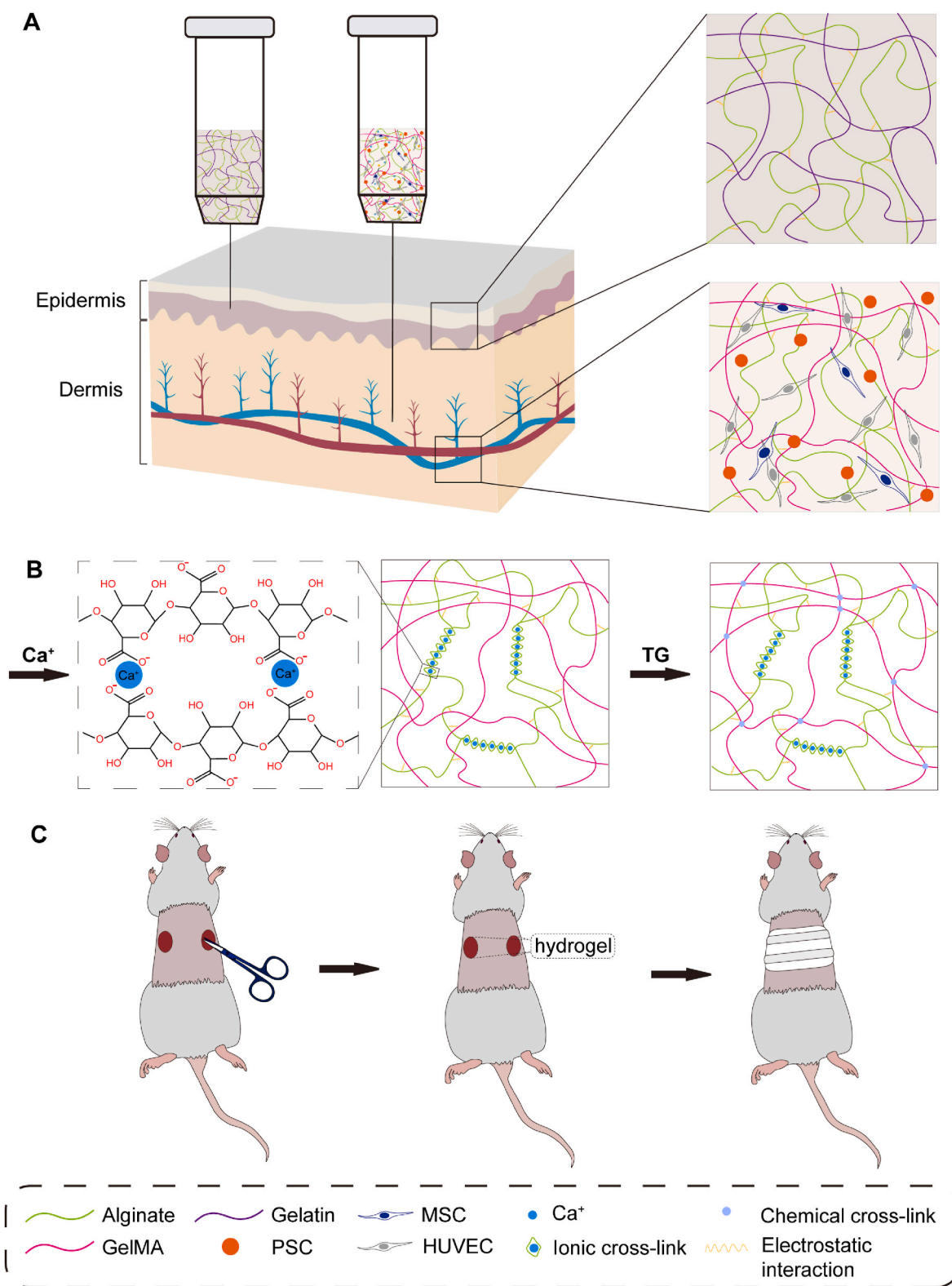
Fig. 1. Schematic diagram of the fabrication process of full-thickness skin substitutes and working principles for the wound healing process. (A) Using 2Alg15Gel and 2Alg3GM5PSC bioinks to print the epidermis layer and the dermis layer, respectively. (B) Physically cross-linking alginate by calcium and chemically cross-linking GelMA or gelatin by TG. (C) The printed full-thickness skin tissues improved angiogenesis activity in the wound bed by embeddingHUVECs, MSCs, and PSC.

that of 2LAlg3GM (2MAlg3GM: 227.725 kPa, 2LAlg3GM: 25.809 kPa). Therefore, medium viscosity sodium alginate was selected, and subsequent experiments were performed.

BG is a promising material that can stimulate angiogenesis in tissue regeneration. As can be seen from its image of SEM (Fig. S1), PSC was

micron-sized. So PSC, a phosphosilicate calcium bioglass, was chosen to improve the performance of hydrogels. Firstly, the microscopic morphology of the mixture hydrogels was observed in Fig. 2D. The SEM images displayed that both 2MAlg3GM and 2LAlg3GM possess micro-sized porous structure, and the pore size increased significantly after
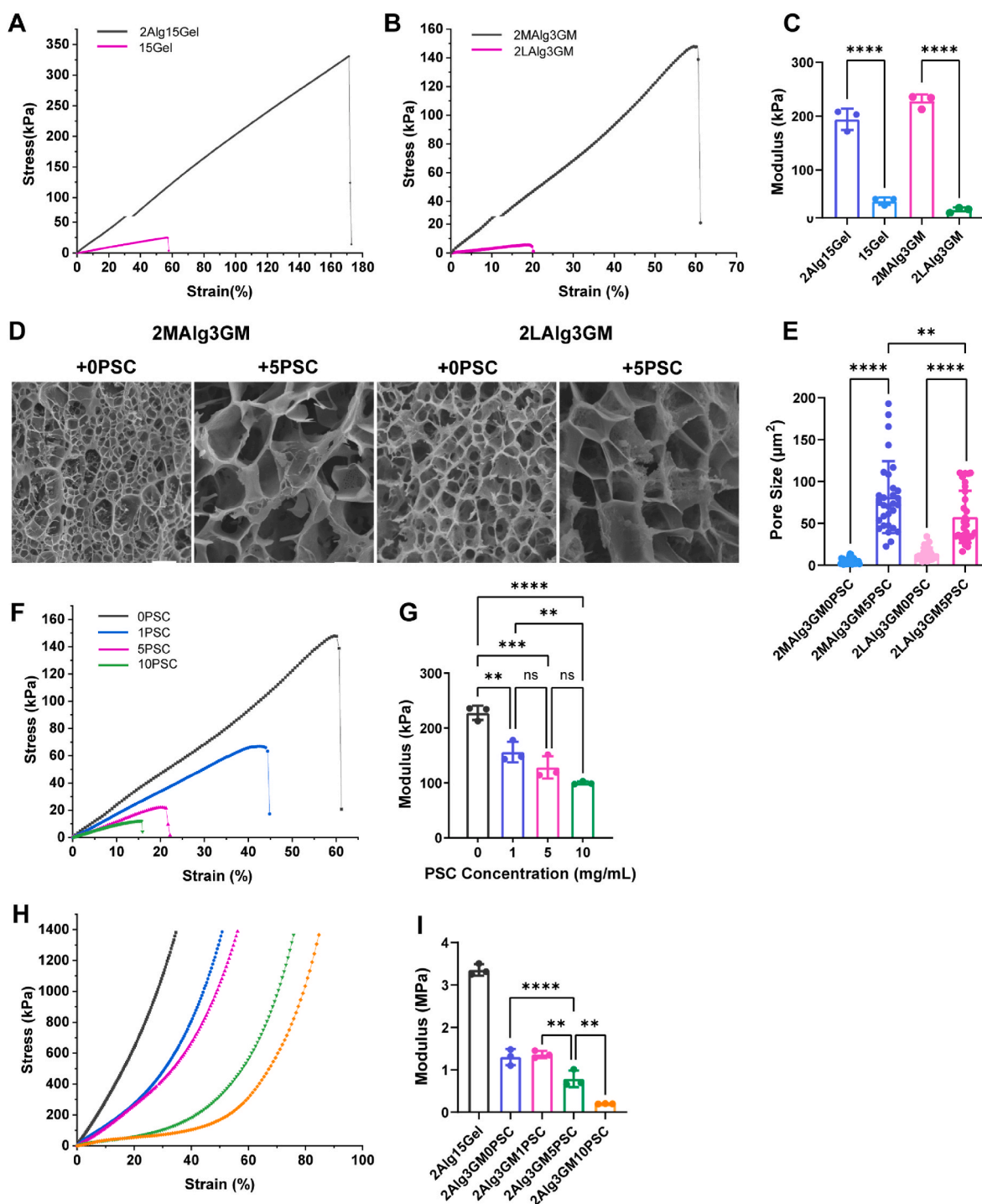
Fig. 2. Morphology and mechanical properties of hydrogel. Tensile stress-strain curves of (A) 2Alg15Gel, 15Gel hydrogels and (B) 2MAlg3GM, 2LAlg3GM hydrogels. (C) Young's modulus of 2Alg15Gel, 15Gel, 2MAlg3GM, and 2LAlg3GM hydrogels (n = 3). (D) Cross-sectional view of SEM images and (E) the average pore size of 2MAlg3GM and 2LAlg3GM hydrogels with and without PSC (n = 3). Scale bars, 5 μm. (F) Tensile stress-strain curves and (G) Young's modulus of 2LAlg3GM hydrogels with 0, 1, 5, and 10 mg mL^{-1} PSC (n = 3). (H) Stress-strain curves of compression testing and (I) compression modulus of 2Alg15Gel, 2LAlg3GM hydrogels with 0, 1, 5, and 10 mg mL^{-1} PSC.

the addition of 5 mg mL^{-1} PSC (Fig. 2E, 2MAlg3GM: 4.430 μm^2, 2LAlg3GM: 81.343 μm^2, 2MAlg3GM5PSC: 13.591 μm^2, 2LAlg3GM5PSC: 57.351 μm^2). Furthermore, PSC were mixed into 2Alg3GM hydrogel in concentrations of 0, 1, 5, and 10 mg mL^{-1} to prepare 2Alg3GM0PSC, 2Alg3GM1PSC, 2Alg3GM5PSC, and 2Alg3GM10PSC hydrogels, respectively. It can be seen from the results that as the concentration of PSCs increased, both the elongation at break (Fig. 2F) and Young's modulus decreased. Although there were significant differences between 0PSC

and each group, there was no significant difference between 5PSC with 1PSC and 10PSC (0PSC: 227.725 kPa, 1PSC: 156.410 kPa, 5PSC: 128.397 kPa, 10PSC: 100.013 kPa). Furthermore, the compression testing results depicted in Fig. 2H and I demonstrate that the modulus of the 2Alg15Gel formulation can attain an impressive value of 3.356 MPa. Similarly, the compression modulus experienced a decline as higher concentrations of PSCs were incorporated. However, even at a PSC concentration of 5 mg/mL, the compression modulus remains notably

robust at 0.789 MPa. Substantial differences in compression modulus were observed between this group and the other three groups, where the values were 1.300 MPa for 0PSC, 1.362 MPa for 1PSC, and 0.204 MPa for 10PSC. Moreover, the addition of PSC would accelerate the degradation of hydrogels, especially when the PSC concentration reaches 5 mg mL^{-1} or more (Fig. S2).

3.2. Characterization of bioinks and printing of full-thickness skin substitutes

To assess the printability of Alg/GM hydrogels in different proportions, viscosity was explored. Firstly, the viscosity of hydrogels consisting of Alg and GM with different weight ratios was compared with the change in shear rate. It was found from Fig. 3A that 5 GM had the best shear thinning performance, but when Alg was mixed with GM, the shear thinning performance was the best when the weight ratio is 1:4 or 2:3. So 2Alg3GM was chosen for subsequent experiments. Furthermore, as the rheological test results shown in Fig. 3B, although all inks had shear thinning performance, it was more significant when 5 mg mL^{-1} and 10 mg mL^{-1} PSC were added. Then, 2Alg3GM5PSC hydrogel was used to choose the appropriate filament orientation from 0° to 90° through printing tests. It was found that the modulus reaches its highest value when filament orientation is 0° (Fig. 3C and D). Due to the instability of structure, the final choice of filament orientation was 60° with the modulus second only to 0° (0°: 288.185 kPa, 30°: 183.951 kPa, 60°: 254.809 kPa, 90°: 159.547 kPa, pouring: 128.397 kPa). Finally, 2Alg15Gel and 2Alg3GM5PSC were used to print the epidermis layer (red) and the dermis layer (green), respectively. A top view, side view, and oblique view of the printed full-thickness skin substitutes were shown in Fig. 3E.

3.3. Biocompatibility and angiogenic activity of bioinks in vitro

Resazurin was used at three specific time points to evaluate the proliferation potential of HFFs and MSCs on 2Alg3GM containing four different concentrations of PSC. It can be seen from Fig. 4A and B, all groups showed a significant increase after culturing for 7 days. The absorbance at 590 nm in all groups was basically similar at each time point, which indicated that the concentrations of PSC did not have much influence on MSCs proliferation. Therefore, four different PSC concentrations were used to culture HFFs, HUVECs, and MSCs for further experimentation.

Furthermore, the full-thickness skin substitute was stained to assess the viability and expression of CD31 on day 1 after printing. The cell viability results (Fig. 4C) showed similar value in every group. So it means that the addition of PSCs does not affect the viability of the cells. However, as the immunofluorescence results illustrated in Fig. 4D and Fig. S3, when the PSC concentration reached 5 mg mL^{-1}, the expression of CD31 increased significantly, and the cells migrated.

After being cultured for 3 days, Q-PCR was used to detect the effects of PSC concentrations on the expression of COL I in HFF, CD31 in HUVEC, and VEGFA in MSC, their primer sequences were shown in Table 1. As the results showed in Fig. 4E and F, and Fig. 4G, cells cultured in hydrogel with 5 mg mL^{-1} PSC expressed the highest growth factor relative gene among all the groups (COL I in HFF, 0PSC: 0.403, 1PSC: 6.599, 5PSC: 19.471, 10PSC: 6.694; CD31 in HUVEC, 0PSC: 4.189, 1PSC: 5.921, 5PSC: 25.478, 10PSC: 10.425; VEGFA in MSC, 0PSC: 32.738, 1PSC: 48.941, 5PSC: 60.544, 10PSC: 24.906). Hence, when the PSC concentration is 5 mg mL^{-1}, it was more favourable for the expression of genes related to angiogenesis.

3.4. Effects of the printed full-thickness skin substitutes in wound healing process in vivo

As shown in Fig. 5, the wound healing effect was assessed by applying 3D bioprinted full-thickness skin substitutes to a full-thickness skin wound in a rat model. The healing of the wound was visually monitored within 2 weeks after different treatments, then photographed
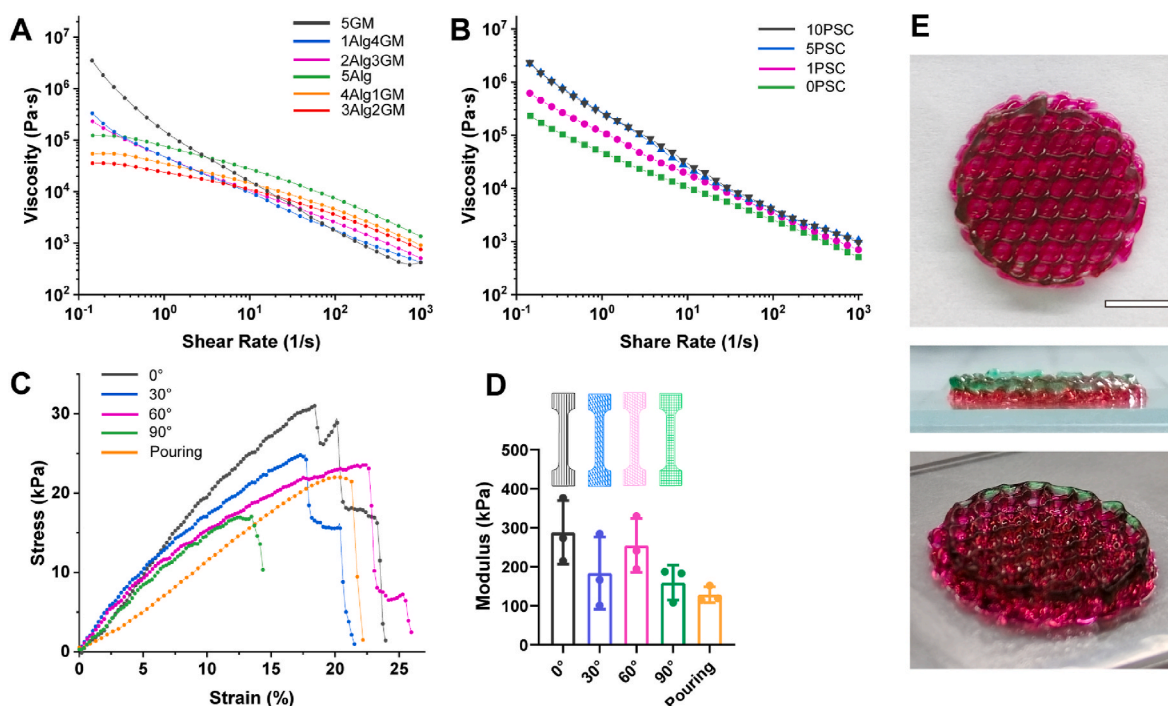

Fig. 3. Rheological properties, mechanical properties of bioinks, and structural properties of the printed full-thickness skin substitutes. Viscosity as a function of shear rate at 10 °C of (A) 5 GM, 1Alg4GM, 2Alg3GM, 3Alg2GM, 4Alg1GM, and 5Alg hydrogels and (B) 2Alg3GM hydrogels with 0, 1, 5, and 10 mg mL^{-1} PSC. (C) Tensile stress-strain curves of the poured or printed dumbbell-shaped molds with 0°, 30°, 60°, and 90° filament orientation (C) and Young's modulus (n = 3). (E) Photograph of the printed epidermis layer (red) and dermis layer (green). Scale bar, 5 mm. (For interpretation of the references to colour in this figure legend, the reader is referred to the Web version of this article.)
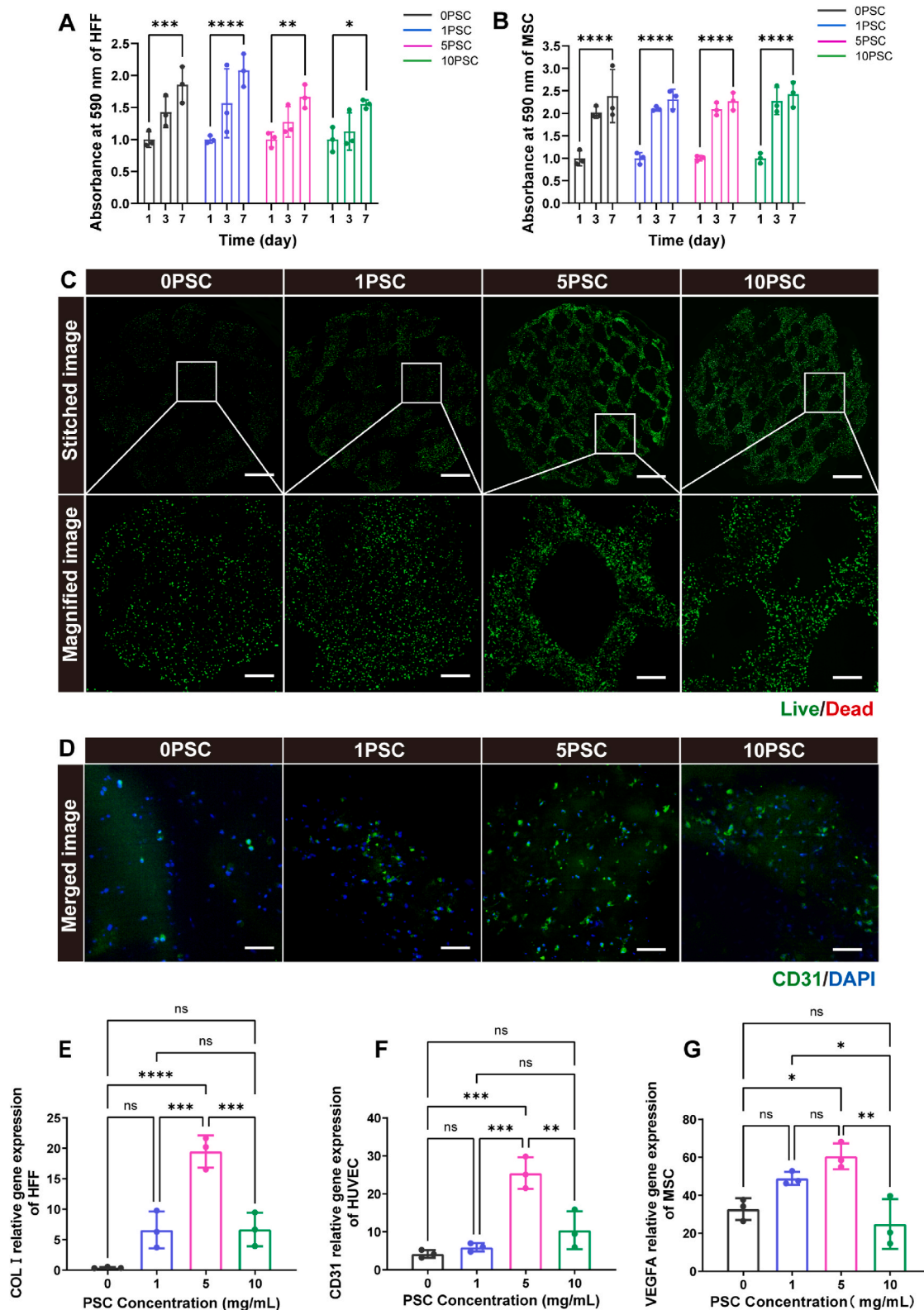
Fig. 4. Cell proliferation, bioactivity, and gene expression *in vitro*. The proliferation of (A) HFFs and (B) MSCs in 2Alg3GM with 0, 1, 5 10 mg mL^{-1} PSC after culturing for 1, 3, and 7 days (n = 3). (C) Live/dead images of HUVECs and MSCs after being printed with 2Alg3GM containing 0, 1, 5 10 mg mL^{-1} PSC for 24 h. Scale bars, 2 mm for stitched images and 400 μm for magnified images. (D) Fluorescence confocal images illustrating the expression of CD31 by MSCs and HUVECs in the bioprinted full-thickness skin substitutes. Counterstain the nuclei with DAPI. Green, CD31; blue, nuclei. Scale bars, 100 μm. The gene expression of (E) COL I in HFFs, (F) CD31 in HUVECs and (G) VEGFA in MSCs (n = 3). (For interpretation of the references to colour in this figure legend, the reader is referred to the Web version of this article.)
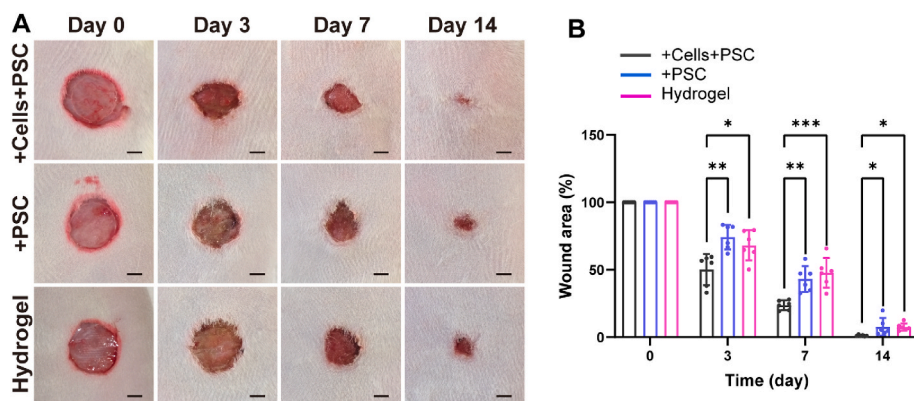
Fig. 5. Evaluation of wound healing of the printed substitutes or hydrogels *in vivo*. (A) Representative pictures of the skin wounds and (B) relative wound area treated with the printed full-thickness skin substitutes (+ Cells + PSC), the printed 2Alg3GM5PSC hydrogels (+PSC), and the printed 2Alg3GM hydrogels (hydrogel) at days 0, 3, 7, and 14 post-surgery (n = 6). Scale bars, 5 mm.
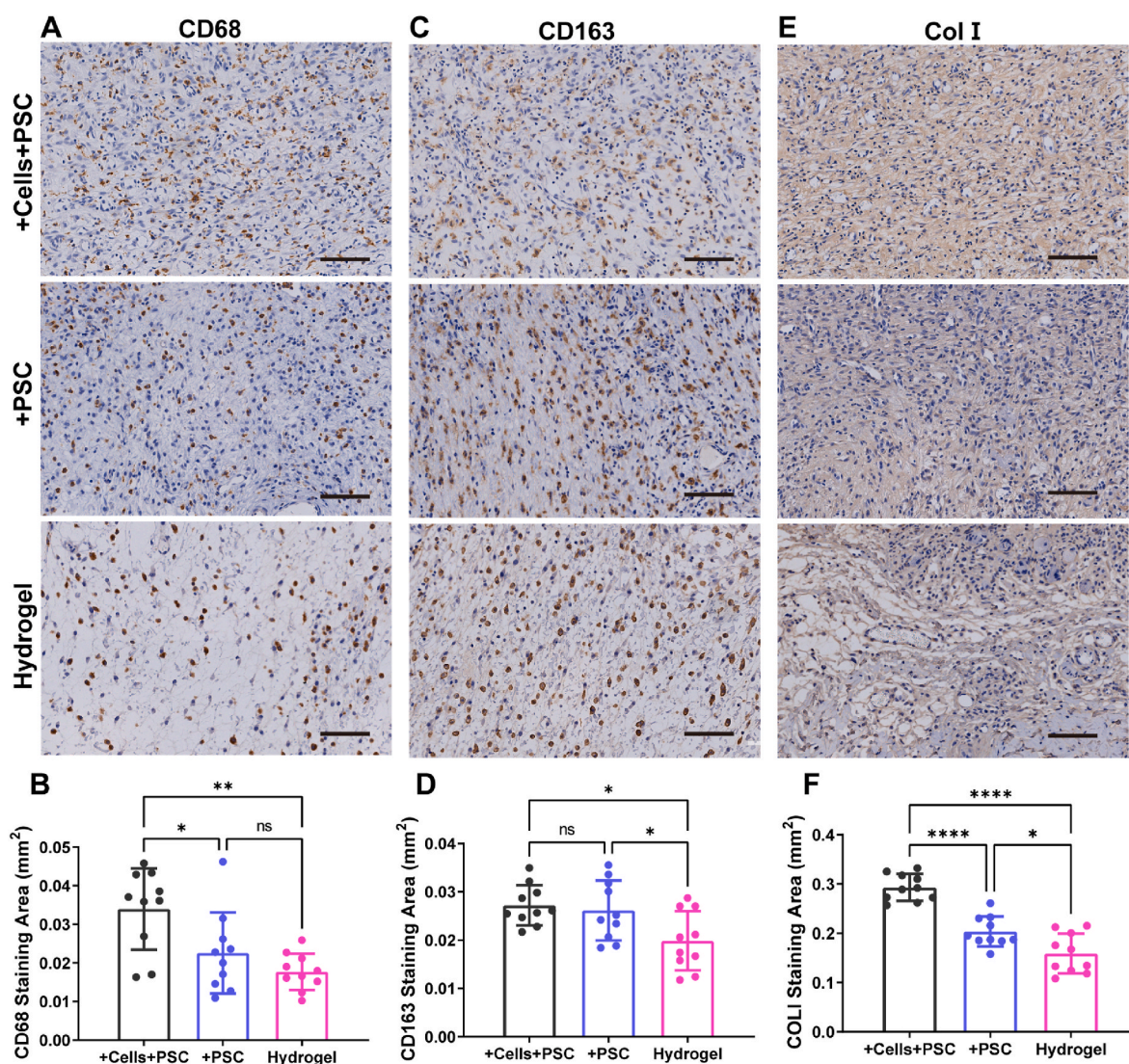

Fig. 6. Histomorphological evaluation of immunoreactivity in wounds. (A) Images of immunohistochemistry staining and (B) its staining area statistics for CD68 (brown) of wound beds treated with the printed full-thickness skin substitutes (+ Cells + PSC), the printed 2Alg3GM5PSC hydrogels (+PSC), and the printed 2Alg3GM hydrogels (hydrogel) at day 3 post-surgery for identifying total macrophages (n = 3). (C) Images of immunohistochemistry staining and (D) its staining area statistics for CD163 (brown) of the wound bed in respective groups at day 7 post surgery for identifying M2 phenotype macrophages (n = 3). (E) Images of immunohistochemistry staining and (F) its staining area statistics for COL I (brown) of wound beds in respective groups at day 14 post surgery (n = 3). Scale bar, 100 μm. (For interpretation of the references to colour in this figure legend, the reader is referred to the Web version of this article.)

and recorded on days 3, 7, and 14 (Fig. 5A). Then the wound closure ability was quantified by the healing time in relation to the wound area (Fig. 5B). At 3 days after surgery, the percentage of wound area varied among different groups. Still, full-thickness substitutes with cells and PSC (+ Cells + PSC) group showed the lowest wound area percentage (+ Cells + PSC: 50.150 %, + PSC: 74.209 %, Hydrogel: 68.122 %). On postoperative day 7, the wound area in the + Cells + PSC group was still the lowest, and the cell-free (+PSC) group was slightly lower than the hydrogel group (+ Cells + PSC: 23.681 %, + PSC: 43.066 %, Hydrogel: 47.749 %). On day 14, the wound of the + Cells + PSC group was basically healed (+ Cells + PSC: 1.142 %, + PSC: 7.584 %, Hydrogel:

7.433 %). In summary, the full-thickness substitutes with cells and PSC group effectively facilitated the wound healing rate and was consistently the highest in all groups at each time point.

The images of immunohistochemical stainings of CD68 and CD163 are shown in Fig. 6A and C, which were markers for macrophages and M2 phenotype macrophages, respectively. It was clear to see that the staining area of CD68 in the + Cells + PSC group was the strongest, while the hydrogel group was the weakest among the three groups at day 3, and this can be easily seen from Fig. 6B (+ Cells + PSC: 0.034 mm^2, + PSC: 0.022 mm^2, Hydrogel: 0.018 mm^2). Interestingly, more M2 phenotype macrophages were observed in the + Cells + PSC group and
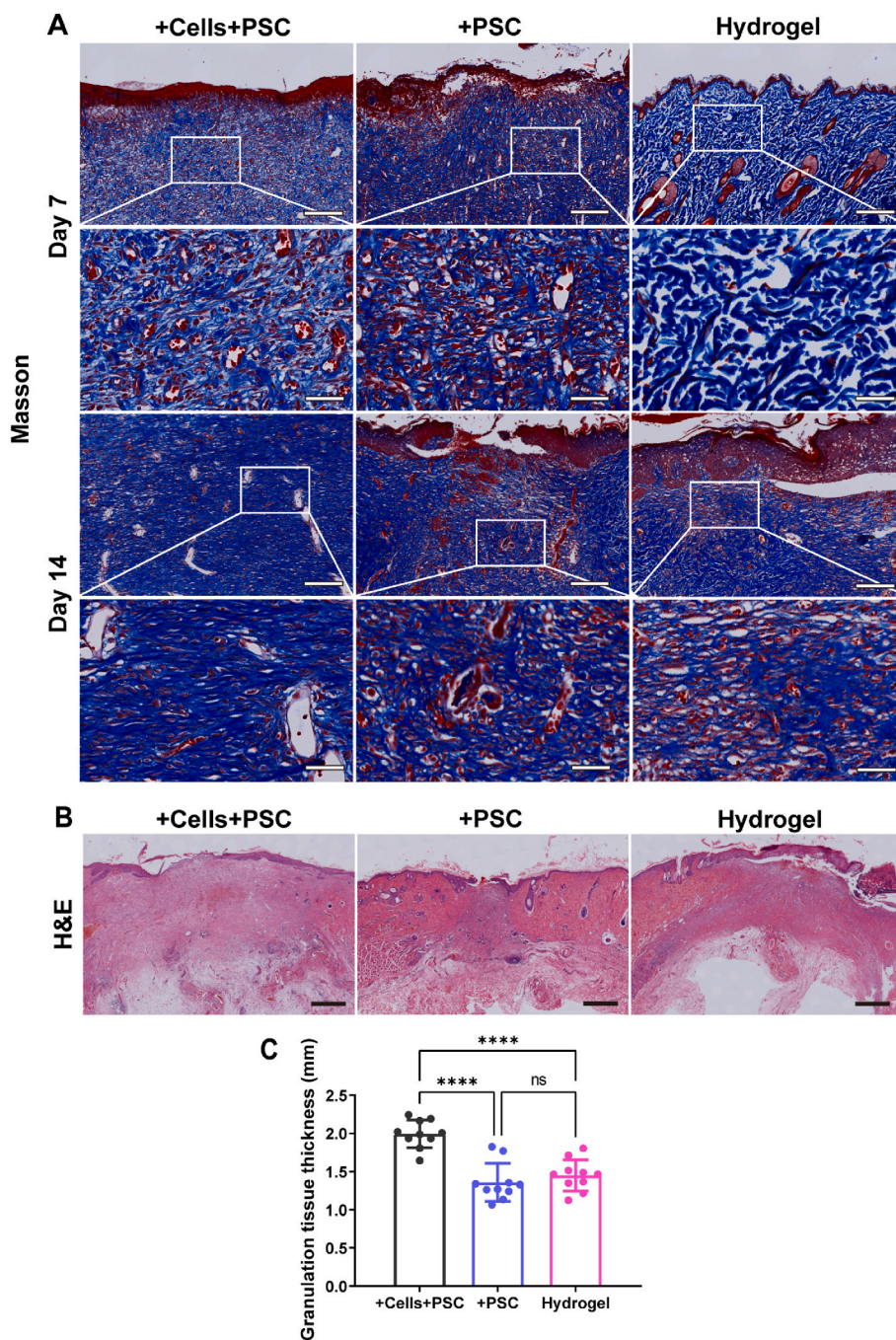

Fig. 7. Microscopic evaluation of wound healing quality. (A) Images of Masson's trichrome staining at days 7 and 14 post-surgery and (B) H&E staining at day 14 post surgery for wound tissues treated with the printed full-thickness skin substitutes (+ Cells + PSC), the printed 2Alg3GM5PSC hydrogels (+PSC), and the printed 2Alg3GM hydrogels (hydrogel). Scale bars, (A) 200 μm for the original view, 50 μm for the close-up view, and (B) 500 μm. (C) Granulation tissue thickness as statistically counted by H&E stained sections in respective groups (n = 3).

the +PSC group on day 7, and the two groups had an almost equal number of M2 macrophages (Fig. 6D) which indicated that PSC promotes the transformation of macrophages to the M2 phenotype (+ Cells + PSC: 0.027 mm^2, + PSC: 0.027 mm^2, Hydrogel: 0.020 mm^2). Furthermore, immunohistochemical staining of COL I was used to confirm the effects of the bioprinted full-thickness skin substitutes on promoting wound healing. As shown in Fig. 8E and F, after 7 days post-surgery, the staining intensity of COL I in the newly formed skin in the + Cells + PSC group was the strongest among these three groups (+ Cells + PSC: 0.293 mm^2, + PSC: 0.204 mm^2, Hydrogel: 0.159 mm^2). Therefore, the + Cells + PSC group stimulated the deposition of COL I in wound areas.

The deposited collagen in wound areas was stained by Masson in blue after treatment for 7 and 14 days with three bioprinted full-thickness skin substitutes. The results are shown in Fig. 7A, which provides information on the deposition and the structure of collagen. On day 7, collagen fibre structure was visible in the wound areas in the + Cells + PSC group, and the collagen fiber density was higher than the other groups. At Day 14, the collagen deposition increased in the wounds, the collagen fibres were thicker, and their arrangement was more closely and orderly than day 7. In addition, larger vascular structures were observed in the + Cells + PSC group.

H&E staining illustrated the representative histological sections of the wound areas in each group after 2 weeks (Fig. 7B). It is clear from the results that, 14 days after surgery, there was already an epidermis and granulation formation in the wound. The results showed that the

granulation tissue in the + Cells + PSC group was significantly thicker than that in the other two groups at day 14 post-surgery (Fig. 7C, + Cells + PSC: 1.994 mm, + PSC: 1.360 mm, Hydrogel: 1.452 mm).

Fig. 8A and B separately illustrated the wound sections detected by CD 31 and α-SMA staining to characterize the vascularization of wound tissue, which was collected from wound areas treated at 14 days. It can be seen that the vessel density and diameter of the + Cells + PSC group were both higher than those of the other two groups. Then the number and diameter of blood vessels were calculated in 15 fields to make a quantitative evaluation. As the statistical results showed, there were significant differences among each groups (Fig. 8C, + Cells + PSC: 39.930, + PSC: 32.730, Hydrogel: 24.670). Furthermore, the diameters of blood vessels in the + Cells + PSC group were much larger than those in other groups (Fig. 8D). In addition, it can be seen from Fig. 8E that the + Cells + PSC group showed the highest density of α-SMA-positive staining cells, and the hydrogel group showed the lowest level (+ Cells + PSC: 0.093 mm^2, + PSC: 0.064 mm^2, Hydrogel: 0.039 mm^2).

4. Discussion

The healing of full-thickness skin defects is currently an urgent problem in clinical treatment. The skin is a combination of two different types of structures—the epidermis and the dermis. Therefore, the skin features suggested that the development of a vascularity ECM covered with a breathable sheath would be a feasible approach in the generation of skin substitutes [30]. The natural wound environment comprises a
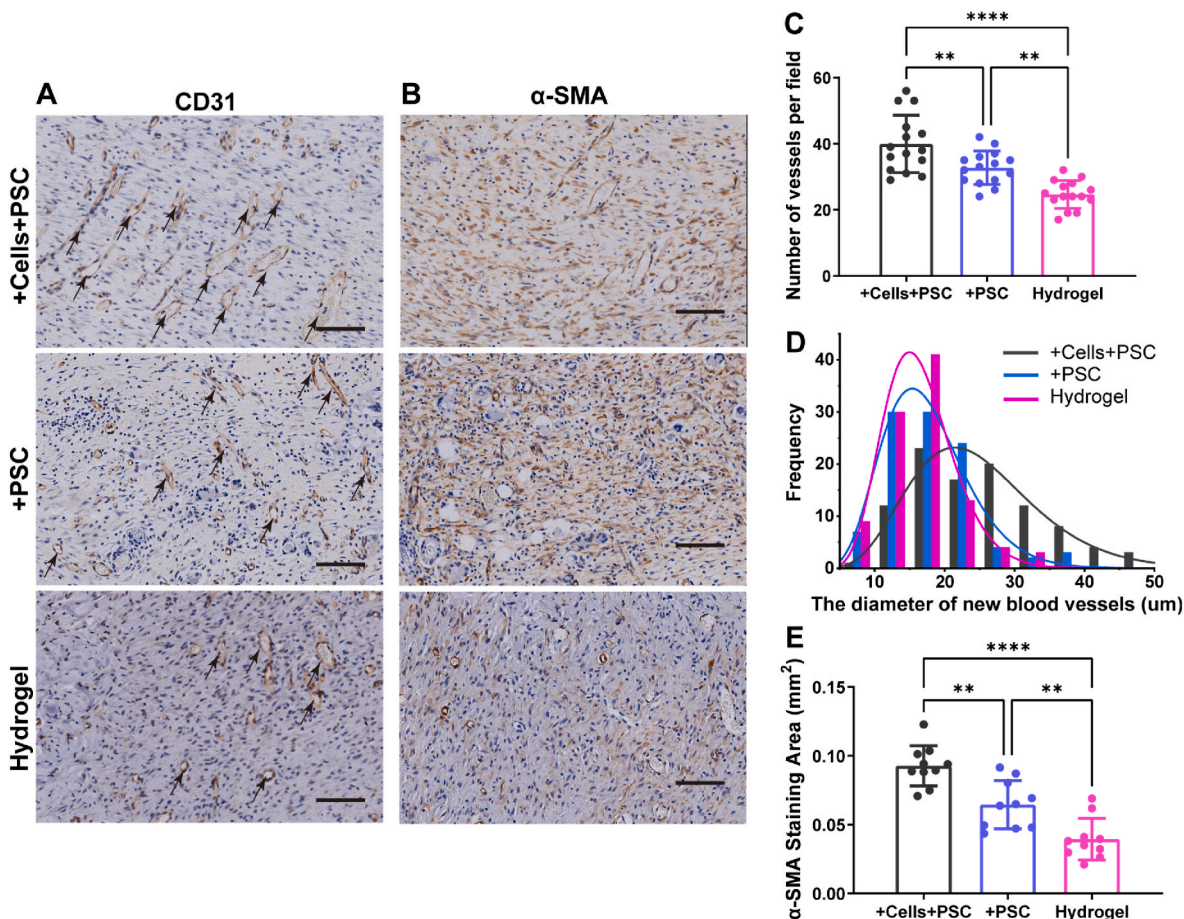

Fig. 8. Histomorphological evaluation of angiogenesis in wounds. Images of immunohistochemistry staining for (A) CD31 (brown) and (B) α-SMA (brown) of wound beds treated with the printed full-thickness skin substitutes (+ Cells + PSC), the printed 2Alg3GM5PSC hydrogels (+PSC), and the printed 2Alg3GM hydrogels (hydrogel) at day 14 post-surgery. Scale bar, 100 μm. Statistics of (C) number of vessels per field (n = 3), (D) diameters of vessels (n = 3), and (E) α-SMA staining area (n = 3) measured from the immunohistochemical images in respective groups. (For interpretation of the references to colour in this figure legend, the reader is referred to the Web version of this article.)

complex composition of an ECM platform with cell adhesive sites, various growth factors, and cells [31]. Replicating the entirety of this microenvironment is a challenging task, which has led to a significant emphasis on designing structural frameworks that play a pivotal role in the healing process.

However, the current state of skin grafts lacks biomimetic mechanical cues that are crucial for promoting vascularization, especially in cases of deeply affected wounds. Additionally, challenges exist in achieving successful integration between the dermal and epidermal layers, as well as ensuring strong adhesion between these layers [32,33]. Commercial skin substitutes available today, such as Integra®, Apligraf®, and Dermagraf®, often come with elevated costs, the risk of requiring two surgeries, and potential complications from infections [34–37]. Consequently, selecting an ideal bioink becomes crucial to strike a balance between mechanical and biological properties that align with the specific requirements of the target tissues. Appropriate mechanical characteristics not only provide temporary support for the lost tissue but also prevent stress concentration at the interface, which could otherwise lead to delamination or hypertrophic scarring [38].

Firstly, to further accelerate wound healing, the formation of new capillary vessels is particularly important, so cells, growth factors, etc. need to be involved [39]. Furthermore, bioactive glass has been widely reported to not only affect cell behaviors but also have the ability to promote angiogenesis [26]. And in our previous study, the provascularizing function of PSC has been verified [40]. Therefore, in this study, we aimed to 3D print an epidermis and dermis contained skin substitute by combining PSC-activated bioinks, endothelial cells, and pericytes.

To print full-tickness skin substitutes and exert excellent wound repair ability, a cytocompatible ink with skin-relevant mechanical properties should be developed. Besides, suitable rheological properties and cell-benign cross-linking are also necessary [41]. With these in mind, sodium alginate, gelatin, and GelMA were chosen for their excellent biocompatibility [42–44]. Moreover, the strong electrostatic interactions between alginate and gelatin, and alginate and GelMA, improve the mechanical properties of a single hydrogel [45]. Then, calcium was used to physically cross-link sodium alginate. TG, a cell-benign enzyme, was used to cross-link gelatin covalently and GelMA [46].

In recent research, Bashiri et al. [47] developed extracellular matrix (ECM)-based bioinks utilizing sodium alginate and gelatin as matrix materials. Their formulation demonstrated optimal prevascularization gene expression upon the addition of 5 % ECM. The resulting bioink exhibited a tensile strength of 0.689 MPa and a compressive strength of up to 1.24 MPa. Similarly, our study utilized a composite hydrogel composed of 2 % Alg and 15 % Gel to emulate the dense and robust epidermal layer. This formulation displayed a tensile modulus of up to 194.234 kPa. Furthermore, the compression testing demonstrated a modulus that can reach 3.356 MPa, thereby contributing significantly to shielding the wound area against external mechanical pressures and impacts [48]. Recently, as studies demonstrated that some bioactive materials possess angiogenic potential [49]. However, direct contact of bioactive glass powder with the wound area often result in a high pH value, which will cause pain in the patient [50]. Thus, PSC, a type of bioactive glass, was embedded in the hydrogel to improve performances of the composite hydrogel of 2 % Alg and 3 % GelMA, mimicking dermis layer and reduce and reduce adverse effects. Although the mechanical properties decreased after adding PSC, the viscosity increased by almost an order of magnitude which was more conducive to extrusion printing. In addition, the design of the filament orientation also further increased the Young's modulus of the full-thickness skin substitute nearly twice as much.

Notwithstanding its therapeutic benefits, the application of pure BG powders usually lead to high pH value in the wound site, which incurs pain to the patients. Most importantly, angiogenesis plays a key role in the process of defect reconstruction. Because skin wounds often result in hypoxia and nutrient depletion, angiogenesis is necessary for wound repair after trauma [22,51]. *In vitro* immunostaining experiments of the bioprinted full-thickness skin substitutes showed that cell migration and CD31 expression were enhanced when the PSC concentration increased. In conclusion, according to the results of the Q-PCR, when the PSC concentration reached 5 mg mL^{-1}, the angiogenic ability was excellently promoted *in vitro*. For example, the expression of COL I and COL III from fibroblasts could also be stimulated, which could accelerate collagen deposition and increase the strength of the wound. Furthermore, it could also stimulate the expression of angiogenesis-related genes, such as CD31 from HUVEC and VEGFA from MSC.

In vivo results illustrated that PSC could promote macrophage secretion and activate M2 phenotype macrophages, as demonstrated through immunohistochemistry staining for CD68 and CD163. In addition, damaged skin needs to restore its function as quickly as possible through the deposition and arrangement of collagen, protecting the host from pathogens [52]. The substitutes + Cells + PSC group promoted collagen I deposition, as seen from the staining for Col I, which was more conductive to attachment, proliferation, and migration of cells [53]. Further, Masson's trichrome staining showed that the substitutes + Cells + PSC group presented the tightest and most orderly collagen arrangement on day 14. Meanwhile, H&E staining showed that the substitutes + Cells + PSC group had thicker and more mature granulation tissue. The angiogenic activity can be directly evaluated by observing new blood vessels *in vivo*. We can see from CD31 staining that more new blood vessels formed after treating with a bioprinted full-thickness skin substitute containing cells and PSC as compared to other groups. Furthermore, the immunohistochemistry staining for α-SMA could also confirm the formation of new blood vessels through staining the smooth muscle cells spread around the new blood vessels.

5. Conclusions

In this study, we utilized bioprinting techniques to create a multi-layer skin substitute that incorporated PSCs. Our findings revealed improved cell proliferation and higher expression of genes associated with angiogenesis *in vitro*. Moreover, *in vivo* experiments demonstrated an enhanced wound healing process, characterized by increased angiogenesis and collagen deposition. Collectively, these results emphasize the promising application prospects of engineering full-thickness skin grafts for effective wound healing.

Author contributions

Q.G. conceived and designed the project together with X.L., Y.L., and X.W.; Y.L., X.L., X.W., and H.G. performed experiments. X.L., Y.L., and Q.G. collected, analyzed the data and wrote the paper.

Declaration of competing interest

The authors declare that they have no known competing financial interests or personal relationships that could have appeared to influence the work reported in this paper.

Data availability

No data was used for the research described in the article.

Acknowledgements

Appendix A. Supplementary data

Supplementary data to this article can be found online at https://doi.org/10.1016/j.mtbio.2023.100899.

References

[1] J.E. Calonje, T. Brenn, A.J. Lazar, S. Billings, McKee's pathology of the skin, 2 volume set E-book, vol. 1, pp. 1–2128, Elsevier Health Sciences (2018).

[2] A.J. Singer, R.A.F. Clark, Cutaneous wound healing, N. Engl. J. Med. 341 (10) (1999) 738–746.

[3] G.C. Gurtner, S. Werner, Y. Barrandon, M.T. Longaker, Wound repair and regeneration, Nature 453 (7193) (2008) 314–321.

[4] V. Falanga, Wound healing and its impairment in the diabetic foot, Lancet 366 (9498) (2005) 1736–1743.

[5] I. Jones, L. Currie, R. Martin, A guide to biological skin substitutes, Br. J. Plast. Surg. 55 (3) (2002) 185–193.

[6] N. Zöller, E. Valesky, M. Butting, M. Hofmann, S. Kippenberger, J. Bereiter-Hahn, A. Bernd, R. Kaufmann, Clinical application of a tissue-cultured skin autograft: an alternative for the treatment of non-healing or slowly healing wounds? Dermatology 229 (3) (2014) 190–198.

[7] D. Chouhan, N. Dey, N. Bhardwaj, B.B. Mandal, Emerging and innovative approaches for wound healing and skin regeneration: current status and advances, Biomaterials 216 (2019), 119267.

[8] S.P. Zhong, Y.Z. Zhang, C.T. Lim, Tissue scaffolds for skin wound healing and dermal reconstruction, Wiley Interdiscip Rev Nanomed Nanobiotechnol 2 (5) (2010) 510–525.

[9] S.V. Murphy, A. Atala, 3D bioprinting of tissues and organs, Nat. Biotechnol. 32 (8) (2014) 773–785.

[10] M. Balasubramani, T.R. Kumar, M. Babu, Skin substitutes: a review, Burns 27 (5) (2001) 534–544.

[11] D.B. Kolesky, R.L. Truby, A.S. Gladman, T.A. Busbee, K.A. Homan, J.A. Lewis, 3D bioprinting of vascularized, heterogeneous cell-laden tissue constructs, Adv. Mater. 26 (19) (2014) 3124–3130.

[12] M.A. Skylar-Scott, J.Y. Huang, A. Lu, A.H.M. Ng, T. Duenki, S. Liu, L.L. Nam, S. Damaraju, G.M. Church, J.A. Lewis, Orthogonally induced differentiation of stem cells for the programmatic patterning of vascularized organoids and bioprinted tissues, Nat. Biomed. Eng. 6 (4) (2022) 449–462.

[13] B.S. Kim, G. Gao, J.Y. Kim, D.W. Cho, 3D cell printing of perfusable vascularized human skin equivalent composed of epidermis, dermis, and hypodermis for better structural recapitulation of native skin, Adv. Healthcare Mater. 8 (7) (2019), e1801019.

[14] J. Ma, C. Qin, J. Wu, H. Zhang, H. Zhuang, M. Zhang, Z. Zhang, L. Ma, X. Wang, B. Ma, J. Chang, C. Wu, 3D printing of strontium silicate microcylinder-containing multicellular biomaterial inks for vascularized skin regeneration, Adv. Healthcare Mater. 10 (16) (2021), e2100523.

[15] S. Michael, H. Sorg, C.T. Peck, L. Koch, A. Deiwick, B. Chichkov, P.M. Vogt, K. Reimers, Tissue engineered skin substitutes created by laser-assisted bioprinting form skin-like structures in the dorsal skin fold chamber in mice, PLoS One 8 (3) (2013), e57741.

[16] N. Hakimi, R. Cheng, L. Leng, M. Sotoudehfar, P.Q. Ba, N. Bakhtyar, S. Amini-Nik, M.G. Jeschke, A. Günther, Handheld skin printer: in situ formation of planar biomaterials and tissues, Lab Chip 18 (10) (2018) 1440–1451.

[17] F.S. Frueh, M.D. Menger, N. Lindenblatt, P. Giovanoli, M.W. Laschke, Current and emerging vascularization strategies in skin tissue engineering, Crit. Rev. Biotechnol. 37 (5) (2017) 613–625.

[18] M. Varkey, D.O. Visscher, P.P.M. van Zuijlen, A. Atala, J.J. Yoo, Skin bioprinting: the future of burn wound reconstruction? Burns Trauma 7 (2019) 4.

[19] J.J. Tomasek, G. Gabbiani, B. Hinz, C. Chaponnier, R.A. Brown, Myofibroblasts and mechano-regulation of connective tissue remodelling, Nat. Rev. Mol. Cell Biol. 3 (5) (2002) 349–363.

[20] P.O. Kwan, E.E. Tredget, Biological principles of scar and contracture, Hand Clin. 33 (2) (2017) 277–292.

[21] F. Urciuolo, C. Casale, G. Imparato, P.A. Netti, Bioengineered skin substitutes: the role of extracellular matrix and vascularization in the healing of deep wounds, J. Clin. Med. 8 (12) (2019).

[22] H. Hu, Y. Tang, L. Pang, C. Lin, W. Huang, D. Wang, W. Jia, Angiogenesis and full-thickness wound healing efficiency of a copper-doped borate bioactive glass/poly (lactic- co-glycolic acid) dressing loaded with vitamin E in vivo and in vitro, ACS Appl. Mater. Interfaces 10 (27) (2018) 22939–22950.

[23] S. Jana, P. Datta, H. Das, P.R. Ghosh, B. Kundu, S.K. Nandi, Engineering vascularizing electrospun dermal grafts by integrating fish collagen and ion-doped bioactive glass, ACS Biomater. Sci. Eng. 8 (2) (2022) 734–752.

[24] S. Zhao, L. Li, H. Wang, Y. Zhang, X. Cheng, N. Zhou, M.N. Rahaman, Z. Liu, W. Huang, C. Zhang, Wound dressings composed of copper-doped borate bioactive glass microfibers stimulate angiogenesis and heal full-thickness skin defects in a rodent model, Biomaterials 53 (2015) 379–391.

[25] F. Bao, G. Pei, Z. Wu, H. Zhuang, Z. Zhang, Z. Huan, C. Wu, J. Chang, Bioactive self-pumping composite wound dressings with micropore array modified janus membrane for enhanced diabetic wound healing, Adv. Funct. Mater. 30 (49) (2020).

[26] H. Yu, J. Peng, Y. Xu, J. Chang, H. Li, Bioglass activated skin tissue engineering constructs for wound healing, ACS Appl. Mater. Interfaces 8 (1) (2016) 703–715.

[27] X. Wang, X. Liu, W. Liu, Y. Liu, A. Li, D. Qiu, X. Zheng, Q. Gu, 3D bioprinting microgels to construct implantable vascular tissue, Cell Prolif. (2023), e13456.

[28] X. Liu, X. Wang, L. Zhang, L. Sun, H. Wang, H. Zhao, Z. Zhang, W. Liu, Y. Huang, S. Ji, J. Zhang, K. Li, B. Song, C. Li, H. Zhang, S. Li, S. Wang, X. Zheng, Q. Gu, 3D liver tissue model with branched vascular networks by multimaterial bioprinting, Adv. Healthcare Mater. 10 (23) (2021), 2101405.

[29] L. Xu, S. Gao, R. Zhou, F. Zhou, Y. Qiao, D. Qiu, Bioactive pore-forming bone adhesives facilitating cell ingrowth for fracture healing, Adv. Mater. 32 (10) (2020), e1907491.

[30] Q. Li, Y. Niu, H. Diao, L. Wang, X. Chen, Y. Wang, L. Dong, C. Wang, In situ sequestration of endogenous PDGF-BB with an ECM-mimetic sponge for accelerated wound healing, Biomaterials 148 (2017) 54–68.

[31] L. Yildirimer, N.T.K. Thanh, A.M. Seifalian, Skin regeneration scaffolds: a multimodal bottom-up approach, Trends Biotechnol. 30 (12) (2012) 638–648.

[32] Y. Guo, J. Huang, Y. Fang, H. Huang, J. Wu, 1D, 2D, and 3D scaffolds promoting angiogenesis for enhanced wound healing, Chem. Eng. J. 437 (2022), 134690.

[33] H. Sorg, D.J. Tilkorn, J. Hauser, A. Ring, Improving vascularization of biomaterials for skin and bone regeneration by surface modification: a narrative review on experimental research 9 (7) (2022) 298.

[34] J.F. Burke, I.V. Yannas, W.C. Quinby Jr., C.C. Bondoc, W.K. Jung, Successful use of a physiologically acceptable artificial skin in the treatment of extensive burn injury, Ann. Surg. 194 (4) (1981) 413–428.

[35] D. Heimbach, A. Luterman, J. Burke, A. Cram, D. Herndon, J. Hunt, M. Jordan, W. McManus, L. Solem, G. Warden, et al., Artificial dermis for major burns. A multi-center randomized clinical trial, Ann. Surg. 208 (3) (1988) 313–320.

[36] W.H. Eaglstein, V. Falanga, Tissue engineering and the development of Apligraf®, a human skin equivalent, Clin. Therapeut. 19 (5) (1997) 894–905.

[37] G.D. Gentzkow, S.D. Iwasaki, K.S. Hershon, M. Mengel, J.J. Prendergast, J. J. Ricotta, D.P. Steed, S. Lipkin, Use of dermagraft, a cultured human dermis, to treat diabetic foot ulcers, Diabetes Care 19 (3) (1996) 350–354.

[38] L. Siebert, E. Luna-Cerón, L.E. García-Rivera, J. Oh, J. Jang, D.A. Rosas-Gómez, M. D. Pérez-Gómez, G. Maschkowitz, H. Fickenscher, D. Oceguera-Cuevas, C. G. Holguín-León, B. Byambaa, M.A. Hussain, E. Enciso-Martínez, M. Cho, Y. Lee, N. Sobahi, A. Hasan, D.P. Orgill, Y.K. Mishra, R. Adelung, E. Lee, S.R. Shin, Light-controlled growth factors release on tetrapodal ZnO-incorporated 3D-printed hydrogels for developing, Smart Wound Scaffold 31 (22) (2021), 2007555.

[39] H. Li, J. Chang, Bioactive silicate materials stimulate angiogenesis in fibroblast and endothelial cell co-culture system through paracrine effect, Acta Biomater. 9 (6) (2013) 6981–6991.

[40] X. Wang, X. Liu, W. Liu, Y. Liu, A. Li, D. Qiu, X. Zheng, Q. Gu, 3D bioprinting microgels to construct implantable vascular tissue, Cell Prolif. 56 (5) (2023), e13456.

[41] D. Wang, S. Maharjan, X. Kuang, L. Mille, L. Tao, P. Yu, X. Cao, L. Lian, L. Lv, J. He, G. Tang, H. Yuk, C. Ozaki, X. Zhao, Y.S. Zhang, Microfluidic bioprinting of tough hydrogel-based vascular conduits for functional blood vessels, Sci. Adv. 8 (2022), eabq6900.

[42] O.D. Frent, L.G. Vicas, N. Duteanu, C.M. Morgovan, T. Jurca, A. Pallag, M. E. Muresan, S.M. Filip, R.-L. Lucaciu, E. Marian, Sodium alginate—natural microencapsulation material of polymeric microparticles, Int. J. Mol. Sci. 23 (20) (2022), 12108.

[43] J. Lei, X. Li, S. Wang, L. Yuan, L. Ge, D. Li, C. Mu, Facile fabrication of biocompatible gelatin-based self-healing hydrogels, ACS Appl. Polym. Mater. 1 (6) (2019) 1350–1358.

[44] M. Xie, Q. Gao, H. Zhao, J. Nie, Z. Fu, H. Wang, L. Chen, L. Shao, J. Fu, Z. Chen, Y. He, Electro-Assisted bioprinting of low-concentration GelMA microdroplets, Small 15 (4) (2019), e1804216.

[45] S.R. Derkach, N.G. Voron'ko, N.I. Sokolan, D.S. Kolotova, Y.A. Kuchina, Interactions between gelatin and sodium alginate: UV and FTIR studies, J. Dispersion Sci. Technol. 41 (5) (2020) 690–698.

[46] C.W. Yung, L.Q. Wu, J.A. Tullman, G.F. Payne, W.E. Bentley, T.A. Barbari, Transglutaminase crosslinked gelatin as a tissue engineering scaffold, J. Biomed. Mater. Res. 83 (4) (2007) 1039–1046.

[47] Z. Bashiri, M. Rajabi Fomeshi, H. Ghasemi Hamidabadi, D. Jafari, S. Alizadeh, M. Nazm Bojnordi, G. Orive, A. Dolatshahi-Pirouz, M. Zahiri, R.S. Kundu, M. Gholipourmalekabadi, 3D-printed placental-derived bioinks for skin tissue regeneration with improved angiogenesis and wound healing properties, Materials Today Bio 20 (2023), 100666.

[48] F. Zhou, Y. Hong, R. Liang, X. Zhang, Y. Liao, D. Jiang, J. Zhang, Z. Sheng, C. Xie, Z. Peng, X. Zhuang, V. Bunpetch, Y. Zou, W. Huang, Q. Zhang, E.V. Alakpa, S. Zhang, H. Ouyang, Rapid printing of bio-inspired 3D tissue constructs for skin regeneration, Biomaterials 258 (2020), 120287.

[49] J. Sonatkar, B. Kandasubramanian, Bioactive glass with biocompatible polymers for bone applications, Eur. Polym. J. 160 (2021), 110801.

[50] Y. Zhu, Z. Ma, L. Kong, Y. He, H.F. Chan, H. Li, Modulation of macrophages by bioactive glass/sodium alginate hydrogel is crucial in skin regeneration enhancement, Biomaterials 256 (2020), 120216.

[51] W. Li, K. Talcott, A. Zhai, E. Kruger, V. Li, The role of therapeutic angiogenesis in tissue repair and regeneration, Adv. Skin Wound Care 18 (2005) 491–500, quiz 501.

[52] D.G. Greenhalgh, The role of apoptosis in wound healing, Int. J. Biochem. Cell Biol. 30 (9) (1998) 1019–1030.

[53] H.P. Lorenz, M.T. Longaker, Wounds: biology, pathology, and management, in: J. A. Norton, P.S. Barie, R.R. Bollinger, A.E. Chang, S.F. Lowry, S.J. Mulvihill, H. I. Pass, R.W. Thompson (Eds.), Surgery: Basic Science and Clinical Evidence, Springer New York, New York, NY, 2008, pp. 191–208.